Regional Attenuation in Northern California: A Comparison of Five 1-D *Q* Methods

by Sean R. Ford, Douglas S. Dreger, Kevin Mayeda, William R. Walter, Luca Malagnini, and William S. Phillips

Abstract The determination of regional attenuation Q^{-1} can depend upon the analysis method employed. The discrepancies between methods are due to differing parameterizations (e.g., geometrical spreading rates), employed datasets (e.g., choice of path lengths and sources), and the methodologies themselves (e.g., measurement in the frequency or time domain). Here we apply five different attenuation methodologies to a Northern California dataset. The methods are: (1) coda normalization (CN), (2) two-station (TS), (3) reverse two-station (RTS), (4) source-pair/receiver-pair (SPRP), and (5) coda-source normalization (CS). The methods are used to measure *Q* of the regional phase, *Lg* (Q_{Lg}), and its power-law dependence on frequency of the form $Q_0 f^{\eta}$ with controlled parameterization in the well-studied region of Northern California using a high-quality dataset from the Berkeley Digital Seismic Network. We investigate the difference in power-law *Q* calculated among the methods by focusing on the San Francisco Bay Area, where knowledge of attenuation is an important part of seismic hazard mitigation. This approximately homogeneous subset of our data lies in a small region along the Franciscan block. All methods return similar power-law parameters, though the range of the joint 95% confidence regions is large ($Q_0 = 85 \pm 40$; $\eta = 0.65 \pm 0.35$). The RTS and TS methods differ the most from the other methods and from each other. This may be due to the removal of the site term in the RTS method, which is shown to be significant in the San Francisco Bay Area. In order to completely understand the range of power-law *Q* in a region, we advise the use of several methods to calculate the model. We also test the sensitivity of each method to changes in geometrical spreading, *Lg* frequency bandwidth, the distance range of data, and the *Lg* measurement window. For a given method, there are significant differences in the power-law parameters, Q_0 and η, due to perturbations in the parameterization when evaluated using a conservative pairwise comparison. The CN method is affected most by changes in the distance range, which is most likely due to its fixed coda measurement window. Since the CS method is best used to calculate the total path attenuation, it is very sensitive to the geometrical spreading assumption. The TS method is most sensitive to the frequency bandwidth, which may be due to its incomplete extraction of the site term. The RTS method is insensitive to parameterization choice, whereas the SPRP method as implemented here in the time-domain for a single path has great error in the power-law model parameters and η is strongly affected by changes in the method parameterization. When presenting results for a given method we suggest calculating $Q_0 f^{\eta}$ for multiple parameterizations using some *a priori* distribution.

Introduction

Measurement of attenuation Q^{-1} of regional seismic phases provides important input for a variety of geophysical applications. It can help with structure and tectonic interpretation (e.g., (Aleqabi and Wysession, 2006; Benz et al., 1997; Frankel, 1990), seismic hazard mitigation through better understanding of strong ground motion attenuation (e.g., Anderson et al. 1996; Hanks and Johnston, 1992), simulation of strong ground motions (e.g., Graves and Day, 2003; Olson and Anderson, 1988), and in nuclear explosion monitoring (e.g., Baker et al., 2004; Mayeda et al., 2003; Taylor et al., 2002). A well-known issue with reported values of Q for regional phases is that they can vary greatly in the same region depending upon the methodology used to derive them. For example, recent one-dimensional (1-D) Q studies in South Korea find frequency-dependent Q of the regional seismic phase, *Lg* (Q_{Lg}), that at 1 Hz range from 450 to 900 (Chung and Lee 2003; Chung et al., 2005). Another example is Tibet where analyses using the same data, but different methods produce a factor of three difference in Q at 1 Hz (McNamara et al., 1996; Xie, 2002). Different data in similar regions in Tibet find a factor of two difference in the power-law dependence that is also dependent on the frequency band in which Q_{Lg} is measured (Fan and Lay 2003a; Xie et al., 2004). Previous work in Northern California has produced best-fit 1-D power-law models ($Q_0 f^n$) of $129f^{0.57}$ (Mayeda et al., 2005) and $105(\pm 26)f^{0.67(\pm 0.16)}$ (Erickson et al., 2004), though, as described below, the focus of this article is not to present a best 1-D Q for Northern California, but rather to document each of the methods and demonstrate a strategy for more reliable determination of Q_0 and its frequency dependence.

In order to reliably use reported Q estimates for other geophysical applications it is essential to know the uncertainty in the estimate. Commonly, individual studies will present aleatoric (random) uncertainty, however epistemic (bias) uncertainty is not possible to assess when only a single method and parameterization is considered. To this end, we implement four commonly applied methods and one new method to measure Q_{Lg}, using a high-quality dataset from the Berkeley Digital Seismic Network (BDSN), in order to better understand the effects of different methods and parameterizations on Q models. The coda normalization (CN) method is implemented in the time domain for paths leading to a common station and it returns a stable Q measurement when the region near a station is homogenous. The coda-source normalization (CS) method uses previously calculated coda-derived source spectra to remove the source term in the frequency domain and is best suited to calculate an effective Q for a given path. The two-station (TS) and reverse two-station (RTS) methods are implemented in the frequency domain and the calculated Q is more stable due to the extraction of the source term. The RTS method produces a power-law Q with less error than the TS method due to its additional extraction of the site terms, though it is more restrictive in its data requirements. The source-pair / receiver-pair (SPRP) method is the RTS method with a relaxation of the data requirements and is implemented in the time domain here. With a more complete knowledge of uncertainty it will be possible to better assess the results of published attenuation studies. Future efforts that employ the multi-method analysis presented here can lead to improved estimates of regional Q.

Data and Methods

We utilize a dataset consisting of 158 earthquakes recorded at 16 broadband (20 sps) three-component stations of the BDSN between 1992 and 2004 (Figure 1, Supplemental Tables). The

wide distribution of data parameters allows for sensitivity testing. We calculate Q_{Lg} by fitting the power-law model, $Q_0 f^n$, using the five different methods. The first two methods, CN and CS, use the seismic coda to correct for the source effect. The last three methods, TS, RTS and SPRP, use a spectral ratio technique to correct for source and, in the case of RTS and SPRP, site effects. In the following we summarize the methods and point out significant differences. Our philosophy in presenting each of the methods is to maintain the approach and style of the commonly applied version of each method as closely as possible. Later, we will attempt to normalize each of the methods for comparison and sensitivity testing. Examples of each method are provided using the control parameterization given in Table 1 and the data used are for paths and stations highlighted in Figure 1.

Coda normalization (CN)

The CN method uses the local shear-wave coda as a proxy for the source and site effects, thus amplitude ratios remove these two effects from the S-wave spectrum (Aki, 1980; Yoshimoto et al., 1993). In his original application, Aki (1980) assumed that the local shear-wave coda was homogeneously distributed in space and time. For the current study region, Figure 1 of Mayeda et al. (2005) shows that the coda at ~1 Hz is in fact homogeneous, at least up to ~240 km. More recently, we have evidence that the high frequencies are also homogeneous and thus the extension of the Aki (1980) method to near-regional distances is warranted. However, the distance limit of the homogeneity assumption has not been fully tested and may manifest in the parameter analysis below. This method assumes the *Lg* amplitude A_{Lg} at a given distance r and frequency f can be estimated by

$$A_{Lg}(f,r) = S(f)R(\theta)I(f)P(f)G(r)\exp\left(\frac{-r\pi f}{QU}\right), \quad (1)$$

where $S(f)$ is the source spectrum and $R(\theta)$ is the source radiation in the source-receiver direction θ. $P(f)$ is the site term, $I(f)$ is the instrument term, and $G(r)$ is the geometrical spreading term, approximated here as

$$G(r) = \left(\frac{1}{r}\right)^{\gamma}, \quad (2)$$

where γ is given in Table 1. The final term is an apparent attenuation, where U is the *Lg* group velocity, which is fixed at 3.5 km/s for this and all other methods. The CN method also assumes that the coda spectrum $C(f)$ is approximately equal to the source spectrum at a given critical propagation time t_C, or

$$C(f,t_C) = S(f)I(f)P(f)E(f,t_C), \quad (3)$$

where $E(f,t_C)$ is a coda excitation term that represents how the spectral amplitude decays with time. The coda excitation term is assumed to be constant at all distances for a given t_C. If the source radiation is smoothed by considering several sources at many source-receiver directions we can take the ratio of A_{Lg} to C, measured at t_C, which effectively removes instrument, site, and

source contributions resulting in the geometrical spreading and attenuation terms. The natural log of this spectral ratio taken at discrete frequency bands (between 0.25, 0.5, 1, 2, 4, and 8 Hz) results in the equation of a line as a function of distance,

$$\ln\left(\frac{A_{Lg}(f)r^{\gamma}}{C(f,t_C)}\right) = \frac{-r\pi f}{QU} + K, \tag{4}$$

where K is the constant derived from the coda excitation factor and the slope is related to Q^{-1}. Q^{-1} at the center frequency of each band then reveals a power-law model for each station.

A_{Lg} is the maximum envelope amplitude in each bandpassed (8-pole acausal Butterworth filter), windowed (according to the window parameter in Table 1) and tapered (10% cosine window) raw vertical trace. C is the root-mean-square (rms) amplitude in each bandpassed 10 second window centered on a t_C of 150 seconds. Data were excluded if either A_{Lg} or C had a SNR less than two, where noise is measured as the maximum amplitude in a window the same length as A_{Lg} prior to the event. This method is similar to that of Chung and Lee (2003), whereas Frankel (1990) used a weighted average of the smoothed coda to measure C. We calculate (4) with all records at a given station, where the slope is calculated with an iteratively weighted least-squares method that reduces the influence of outlier observations. An example for station PKD is given in Figure 2. The resulting Q^{-1} are then fit in the log domain as a function of midpoint frequency with a weighted (the squared inverse of the standard error in each Q^{-1} measurement) least-squares line to calculate the power-law parameters (Figure 2b). We bootstrap the residuals of the weighted fit 1000 times with replacement to calculate standard error of the power-law parameters. This bootstrapping method randomly adds the residuals of the inversion to the fit and repeats the inversion. The procedure is repeated n times with replacement, and variance in the fit parameters can be extracted from the empirical covariance matrix calculated from the model parameter population of size n (Aster et al., 2004; Moore and McCabe, 2002). Resampling more than 1000 times introduced no additional variation.

Coda-source normalization (CS)

The CS method uses the stable, coda-derived source spectra to isolate the path attenuation component of the *Lg* spectrum (Walter et al., 2007). This method assumes A_{Lg} is represented as in equation (1) with $S(f)$ described as in Aki and Richards (2002),

$$S(f) = \frac{\dot{M}(t)}{4\pi\sqrt{\rho_s\rho_r\beta_s\beta_r\beta_s^2}}, \tag{5}$$

where $\dot{M}(t)$ is the moment-rate time function, and ρ and β are the density and velocity of the medium near the source, s, and receiver, r, respectively. We use an average ρ of 2600 kg/m^3 and β of 3000 m/s near both the source and receiver. $R(\theta)$ is fixed at 0.6, the absolute value average of the radiation pattern for a double-couple (Boore and Boatwright, 1984). $G(r)$ is a critical distance formulation (Street et al., 1975),

$$G(r) = \begin{cases} r^{-1} & \text{for } r < r_0 \\ \frac{1}{r_0}\left(\frac{r_0}{r}\right)^{\gamma} & \text{for } r \geq r_0 \end{cases}, \quad (6)$$

where γ is given in Table 1. We fix r_0 at 60 km, which is two times an approximate crustal thickness for the region. We assume a site term $P(f)$ of unity and thus any site effect is projected into the path attenuation term.

The windowed (according to the window parameter in Table 1) and tapered (10% cosine window) transverse component is transferred to velocity and its Fourier amplitude is calculated. A_{Lg} is then the mean of the Fourier amplitude for fixed discrete frequency bands (between 0.2, 0.3, 0.5, 0.7, 1, 1.5, 2, 3, 4, 6, and 8 Hz). Path attenuation can then be extracted with the log transform via

$$Q(f) = \frac{\left(r\pi f \log(e)/U\right)}{\log\left(S(f)\right) + \log\left(G(r)\right) + \log\left(P(f)\right) - \log\left(A_{Lg}(f)\right)}, \quad (7)$$

where the same frequency bands are used to calculate the source spectra, $S(f)$, and $P(f)$ is fixed to unity. Source spectra derived from the coda are calculated via the methodology of Mayeda et al. (2003) and are from the Northern California study of Mayeda et al. (2005). $Q(f)$ is only calculated for records where A_{Lg} is two times the amplitude of the pre-event signal (SNR > 2). Q at the center frequency of each band then reveals a power-law model for each event-station path.

We fit a least-squares line in the log domain (a robust regression gave similar results) and require the correlation of the fit be positive and the correlation coefficient be nonzero with a high degree of confidence ($p < 0.05$). The intercept term is then the log transform of Q_0 and the slope is η (Figure 3). We bootstrap the residuals of the fit to calculate standard error of the power-law parameters as described in the CN method.

Two-station (TS)

The TS method takes the ratio of *Lg* recorded at two different stations along the same narrow path from the same event in order to remove the common source term (e.g., Chavez and Priestley, 1986; Xie and Mitchell, 1990). We implement this method in the frequency domain and take the ratio of two terms with the form of equation (1), which gives

$$\frac{A_{Lg}^1(f)}{A_{Lg}^2(f)} = \frac{S(f)R(\theta)I^1(f)P^1(f)G(r_1)}{S(f)R(\theta)I^2(f)P^2(f)G(r_2)}\exp\left(\frac{(r_2 - r_1)\pi f}{QU}\right), \quad (8)$$

where the superscripts refer to station 1 or 2 and $r_1 < r_2$. If we assume the ratio of the site terms ($P^1(f)/P^2(f)$) to be near unity we can use the natural log transform of equation (8) to obtain

$$\alpha(f) = \frac{U}{\pi(r_2 - r_1)} \ln\left(\frac{A_{Lg}^1}{A_{Lg}^2} \left(\frac{r_1}{r_2} \right)^{\gamma} \right) = \frac{f^{(1-\eta)}}{Q}, \tag{9}$$

assuming a power-law model for attenuation and $G(r)$ as in equation (2). A_{Lg} is the Fourier amplitude spectra of the windowed (according to the window parameter in Table 1) and tapered (10% cosine window) vertical component that has been transferred to velocity. We only calculate ratios where the smoothed (moving average of 0.4 Hz) Fourier amplitude ratio of A_{Lg} to pre-event signal is greater than two (SNR > 2), and where $\alpha(f)$ is directly proportional to frequency. We limit the azimuthal gap between stations and event to 15°.

$\alpha(f)$ is decimated so that the frequency step Δf is

$$\Delta f = \frac{f_{Nyq}}{L}, \tag{10}$$

where f_{Nyq} is the Nyquist frequency of the A_{Lg} time-series and L is the number of points. This is done so that $\alpha(f)$ represents the resolution of the discrete Fourier transform. Equation (8) can be transformed to the log-domain and a linear regression is possible to calculate the power-law parameters. However, random error due to propagation can produce a negative $\alpha(f)$ at some frequencies (Xie, 1998), which prohibits analysis in the log-domain. Figure 4 illustrates this effect. Therefore, we perform a non-linear regression on $\alpha(f)$ that minimizes the sum of squares error on the power-law function in the least-squares sense (Bates and Watts, 1988). We bootstrap the residuals of the non-linear fit to calculate standard error of the power-law parameters as described in the CN method, where the inversion is done non-linearly.

Reverse two-station (RTS)

The RTS method uses two TS station-event configurations and forms a ratio of two equations of the form of (8), where a source is on either side of the station pair in a narrow azimuthal window (Chun et al., 1987). The two ratios are combined to remove the common source and site terms to give

$$\alpha(f) = \frac{U}{\pi(r_2 - r_1 + r_4 - r_3)} \ln\left(\frac{A_{Lg}^1 A_{Lg}^3}{A_{Lg}^2 A_{Lg}^4} \left(\frac{r_1 r_3}{r_2 r_4} \right)^{\gamma} \right) = \frac{f^{(1-\eta)}}{Q}, \tag{11}$$

where $r_2 > r_1$ and $r_4 > r_3$ and $G(r)$ as in equation (2). $\alpha(f)$ is calculated similarly to the TS method. Figure 5 shows an example of the RTS method for the same interstation path as the TS example given in Figure 4. The RTS method reduces the variance of $\alpha(f)$.

Source-pair/receiver-pair (SPRP)

The SPRP method is the RTS method with a relaxation on the narrow azimuthal window requirement (Shih et al., 1994). We implement this method in the time domain so that equation (11) becomes

$$\ln\left(\frac{A_{Lg}^1 A_{Lg}^3}{A_{Lg}^2 A_{Lg}^4}\left(\frac{r_1 r_3}{r_2 r_4}\right)^{\gamma}\right) = \frac{\pi f}{QU}(r_2 - r_1 + r_4 - r_3). \quad (12)$$

Unlike the RTS method, data are no longer restricted by a given azimuth, but by a distance formulation

$$r_A^2 > (SP^2 + r_B^2), \quad (13)$$

where the subscript A refers to the larger epicentral distance records (r_2 and r_4) and B refers to the smaller distance records (r_1 and r_3), and SP is fixed at 50 km (Chung et al., 2005). This gives an effective maximum azimuthal gap at some interstation distances of 70°. A_{Lg} is the maximum zero-to-peak amplitude in each bandpassed (8-pole acausal Butterworth filter), windowed (according to the window parameter in Table 1) and tapered (10% cosine window) vertical component record that has been transferred to velocity. The left side of equation (12) is least-squares fit as a function of the effective interstation distance, (r_2 - r_1 + r_4 - r_3), for the same discrete frequency bands as in the CN method, where f is the midpoint of these frequency bands (Figure 6a). We require the correlation of the fit be positive and the correlation coefficient be nonzero with a high degree of confidence ($p < 0.05$). The slope of the fit is a function of Q^{-1} in the band that it was measured. The resulting Q^{-1} are then fit in the log domain as a function of midpoint frequency with a weighted (the squared inverse of the standard error in each Q^{-1} measurement) least-squares line to calculate the power-law parameters (Figure 6b). Standard error in the power-law parameters is from the covariance matrix estimated from the residuals.

We note that in the example calculation given in Figure 6, where Q_{Lg} is estimated between stations PKD and SAO, that Q^{-1} between 1 and 2 Hz in Figure 6a is so small as to not be a visible data point on Figure 6b. The available data does not support a stable calculation of the power-law parameters in this case. The instability is due to a small sub-population of data centered at an effective distance of 150 km. These data are due to an event that has a difference in azimuth between stations of 26°. This effect illustrates a pitfall of this method whereby, although more data is made available, the paths to each station may not be along a narrow azimuth and will sample a structure that is different along paths and no longer directly between stations.

Method comparison

Since each method has a different data requirement it is inappropriate to compare the methods with the full dataset. For example, the CN method will sample geology at all back-azimuths relative to a station, whereas the RTS method is restricted to a narrow azimuthal window aligned roughly along a pair of stations and events. In an attempt to normalize the dataset used for each method, we restrict the data to lie in a small region along the Franciscan block (Figure 7a).

We implement all five methods to calculate $Q_0 f^n$ in the region using the Control parameterization given in Table 1 (Figure 7b). Equation (4) of the CN method is calculated and regressed for all epicentral distances in the region. The Q^{-1} and their standard errors are then put into a weighted least-squares as above, where the residuals are bootstrapped 1000 times to produce a population

of power-law parameters. This population is then smoothed with a two-dimensional Gaussian kernel (Venables and Ripley, 2002) to produce an empirical probability density so that the 95% confidence region can be estimated. Equation (7) of the CS method is calculated for all event-station paths in the region. In order to get at the true variability in the region, we create 1000 subsets of these paths by randomly selecting one member of each Q population for a given discrete frequency band at all frequencies. This new subset is then least-squares fit in the log-domain to find the power-law parameters. We find the empirical distribution as described previously and estimate a 95% confidence region. A similar method is employed for the TS and RTS methods. All $\alpha(f)$ from equations (9) or (11) are calculated for the region and 1000 subsets are produced by randomly selecting one member of each α population for a given frequency. This subset is then fit with the same non-linear squares method as described above to produce an empirical distribution of power-law parameters where a 95% confidence region can be estimated. The SPRP method is carried out similarly to the CN method. This is a more appropriate implementation of this method, as compared to a single interstation path, since now a more even distribution of effective interstation distances can be used.

Figure 7b shows that the range in Q_0 (~30) and η (~0.5) are similar for all methods, though the mean of the empirical population distribution is not always the same. This difference is most evident between the RTS and TS methods, which differ in the RTS method's ability to remove the site terms. The different parameter means may suggest that the site term has a considerable effect on attenuation in the region, and this effect will be discussed below. Except for the TS method, all methods retrieve a similar mean Q_0, where the mean η for the RTS method differs from the other methods by just ~0.15. Using the limits for all the methods, the 1-D model parameters in the region vary between 40 and 125 for Q_0, and 0.3 and 1.0 for η. The grey region in Figure 7b represents a parameter space that fits all method parameter distributions, where Q_0 is between 70 and 95, and η is between 0.5 and 0.7.

Sensitivity tests

Using the complete dataset, we investigated how the choice of parameterization affects the results. In each test, only one parameter was varied, and $Q_0 f^{\eta}$ was calculated with each of the methods. The varied parameters are geometrical spreading rate (γ), measurement bandwidth, epicentral distance, and the *Lg* window. The values of the varied parameters are listed in Table 1, where the range was chosen based on values used in previous studies.

For the CN method, standard error regions were constructed from the covariance of the power-law model parameters estimated by bootstrapping the residuals of the weighted least-squares fit 1000 times. Figure 8a shows the standard error regions for each test at station PKD. All tests cluster around the control parameters except the distance test (Test 3). To assess the significance of model parameterization differences we perform an analysis of covariance (ANCOVA) for the weighted least-squares regression with Tukey's honest significant difference (HSD) pairwise comparison tests (Faraway, 2004). This pairwise comparison method finds a significant difference in the model parameters only if the 95% confidence region of the mean difference in the model parameters between the test and control does not include zero. The HSD test is more appropriate than a t-test when comparing more than one group, as is done here between the control and four tests. We group all significant differences between a given test and the control

parameterization and plot the median and 25th and 75th percentile values of that group, while noting the percentage of stations that had significant differences for each test (Figure 8b). In this way, we can try and separate aleatoric uncertainty due to poorly constrained power-law model parameters and epistemic uncertainty due to the choice of parameterization for each method. Therefore, the confidence regions in panel a) of Figures 8-12 can be interpreted as the aleatoric uncertainty, and the values in panel b) as epistemic uncertainty. There is a significant difference for almost all CN method comparisons in η, and the greatest difference for both model parameters is when the epicentral distance of the dataset is changed (Test 3). This is due to the fixed time t_C at which the coda is measured, where for greater distances it may be more appropriate to increase t_C, or relate its value to the *S*-wave velocity.

Standard error regions and pairwise comparisons are calculated for the CS method as described above, though the residuals and ANCOVA are for a direct linear regression (Figure 9). For most Tests only a small fraction of the comparisons are significantly different. However, when γ is changed in equation (7) (Test 1) there is a significant difference in Q_0 for 39% of the path comparisons, where the median difference is almost 50. This effect highlights the difficulty in extracting an intrinsic Q from the full path attenuation when examining a single path. The CS method is best for evaluating the total path term $P(f)G(r)\exp(-r\pi f/QU)$ from equation (1).

Since the TS and RTS methods require nonlinear regressions, we estimate covariance matrices from the bootstrapped power-law model parameter populations. ANCOVA is performed with this estimated covariance and the pairwise comparisons are made with the results (Figure 10-Figure 11). A change in epicentral distance does not significantly affect the power-law parameters for both the TS and RTS methods, but a change in bandwidth (Test 2) produces an interquartile range of 0.05 to 0.22 for the difference in η using the TS method. The TS method is sensitive to site effects and this difference may be due to site effects that are different below 1 Hz than they are above it. For several stations in the BDSN this seems to be the case (Malagnini et al., 2007). The RTS method doesn't suffer from this same dependency and its median significant differences are low for all Tests.

As previously stated, the SPRP method implemented in the time domain requires a distribution of effective interstation distances that can best be given when several interstation paths are considered. However, it should be able to constrain $Q_0 f^{\eta}$ for a single interstation path, and in order to allow for comparison with the implementation of the other interstation methods, TS and RTS, we carry out the method on an interstation basis. The effects of this suboptimal design are evident in the aleatoric error shown for the example path from PKD to SAO in Figure 12a, where the standard error regions are very large. Due to such large standard error regions only approximately half of the pairwise comparisons give a significant difference in Q_0. However, the same comparisons reveal a large difference in η for all but the γ Test (Test 1).

Discussion

Each method analyzed here is employed for different types of investigations. Table 2 displays the advantages, disadvantages and assumptions of the methods. The CN method returns a stable Q measurement when the region near a station is homogenous, and could be easily implemented in a tomographic inversion scheme.

The CS method is best suited to calculate an effective Q for a given path, where the site term is mapped into the path attenuation. Also, since it measures the path directly from the event to station, there is a trade-off between geometrical spreading and effective Q. If the uncertainties in the type of geometrical spreading are large, then it may be best to test several forms of spreading, or to fold the spreading term into the entire path effect if this is appropriate for the application.

The TS and RTS methods are more stable due to the extraction of the source term. The RTS method produces the least error due to its additional extraction of the site terms, though it is more restrictive in its data requirements. Xie (2002) calculates the bias due to the site term assumption in the TS method and finds that it is small. In order to test this assumption and gain more insight to the differences present in Figure 7, we compare the power-law parameters calculated with the TS method for interstation paths with station BKS and those from a nearly co-located BRK. Malagnini et al. (2007) find a significant difference in the site term between BKS and BRK and this difference is evident in Figure 13, where several of the paths do not fall along the $x=y$ line. However, the difference in site effect between BKS and BRK is likely to be an extreme case for the BDSN, since BKS is in highly fractured rock near the Hayward Fault.

The SPRP method is the RTS method with a relaxation of the data requirements and is appropriate for very laterally homogeneous Q. The SPRP method is implemented in the frequency domain by Fan and Lay (2003b) and in the time domain by Shih et al. (1994) and Chung et al. (2005) where they find clusters in small regions that are very different from the overall 1-D Q model. The SPRP method in the time domain is much better suited for a large homogeneous region, where several interstation regions can be grouped together. Not grouping regions may result in pooling of data points near the true interstation distance. This can greatly effect the linear regression and produce large error in the model parameters. Such an effect can be seen in the example in Figure 6. However, this effect could be lessened by the use of a moving-average filter, though this could result over-weighting some points. The SPRP method requires the use of several interstation paths so a tectonically stable area is needed.

Much of the variation in 1-D power-law model parameters shown in Figure 7 may be due to structural heterogeneity in the region. In fact, a similar range in Q can be seen in the same Northern California subregion in Figure 2 of Mayeda et al. (2005). However, there are differences in the model parameter populations in Figure 7, and in order to fully understand epistemic uncertainty of a regional model we advise the use of several methods to estimate parameters.

The parameterization choices can greatly affect the calculated power-law Q model. Therefore, knowledge of appropriate distributions of these parameters can help reduce the variance in the model and produce more realistic Q models. The geometrical spreading considered for a given method can have direct trade-offs with Q (Atkinson and Mereu, 1992; Bowman and Kennett, 1991). Nuttli (1973) and Campillo et al. (1985) model the geometrical spreading exponent (γ, in this study) in the time domain to be 5/6 (~0.83). However, Yang (2002) shows that a more appropriate time domain assumption when measuring the *Lg* rms amplitude is 1. Spreading in the frequency domain is more stable and 0.5 is a robust estimate, and is what Street et al. (1975) assumes past a given critical distance. Future work should use an appropriate range of spreading

in the time domain and some distribution of γ in the frequency domain. The appropriate group velocity window can also affect the 1-D Q model. Campillo (1990) uses synthetic tests to show that earlier energy in a given *Lg* window samples the shallow crust, whereas later arriving *Lg* energy has sampled a larger portion of the crust. Producing power-law Q from a range of windows within the observed *Lg* energy window could illuminate this effect and aid in the derived model interpretation.

Conclusions

We apply the coda normalization (CN), two-station (TS), reverse two-station (RTS), source-pair/receiver-pair (SPRP), and the new coda-source normalization (CS) methods to measure Q_{Lg} and its power-law dependence ($Q_0 f^{\eta}$) in northern California in order to understand the variability due to parameterization choice and method. We investigate the reliability of the methods by comparing them with each other for an approximately homogeneous region in the Franciscan block near the San Francisco Bay Area. All methods return similar ranges in power-law parameters when considering the 95% confidence regions. The joint distribution using all methods gives $Q_0 = 85 \pm 40$ and $\eta = 0.65 \pm 0.35$ (both ~95% CI). However, the centers of the RTS and TS method distributions differ from each other, though the mean Q_0 of the RTS method is similar to those of the other three methods. This may be due to the removal of the site terms for the RTS method, which suggests that when site effects are not uniform within a region several 1-D methods should be employed in order to assess the full range of models.

We test the sensitivity of each method to changes in geometrical spreading, *Lg* frequency bandwidth, the distance range of data, and the *Lg* measurement window. For a given method, there are significant differences in the power-law parameters, Q_0 and η, due to perturbations in the parameterization when evaluated using a conservative pairwise comparison. The CN method is affected most by changes in the distance range, which is likely due to its fixed coda measurement window or the fact that at larger distances the coda is not homogeneously distributed. Since the CS method is best used to calculate the total path attenuation, it is very sensitive to the geometrical spreading assumption. The TS method is most sensitive to the frequency bandwidth, which may be due to its incomplete extraction of the site term. The RTS method is insensitive to parameterization choice, whereas the SPRP method as implemented here in the time-domain for a single path has great error in the power-law model parameters and η is greatly affected by changes in the method parameterization. When presenting results for a given method it is best to calculate $Q_0 f^{\eta}$ for multiple parameterizations using an *a priori* distribution.

Acknowledgements

Figures were made with GMT (Wessel and Smith, 1998). Signal processing was done with SAC (Goldstein et al., 1999). Some statistical analysis was done with R (R Development Core Team 2006). This research is sponsored by the Department of Energy through the National Nuclear Security Administration, Office of Nonproliferation Research and Development, Office of Defense Nuclear Nonproliferation. This research was performed under the auspices of the U.S. Department of Energy by the University of California Lawrence Livermore National Laboratory under contract number W-7405-ENG-48. This is LLNL contribution UCRL-JRNL-233738. BSL #. L.M. was partially supported by project "Stima dello scuotimento in tempo reale e quasi-reale

per terremoti significativi in territorio nazionale", funded by Dipartimento della Protezione Civile (DPC).

References

Aki, K., and P. G. Richards (2002). Quantitative seismology, Sausalito: University Science Books.

Aki, K. (1980). Attenuation of shear-waves in the lithosphere for frequencies from 0.05 to 25 Hz, *Phys. Earth Planet. Inter.* **21,** 50-60.

Aleqabi, G. I., and M. E. Wysession (2006). *Q*(*Lg*) distribution in the basin and range province of the western United States, *Bull. Seis. Soc. Amer.* **96,** 348-354.

Anderson, J. G., Y. Lee, Y. Zeng, and S. Day (1996). Control of strong motion by the upper 30 meters, *Bull. Seis. Soc. Amer.* **86,** 1749-1759.

Aster, R., B. Borchers, and C. H. Thurber (2004). Parameter estimation and inverse problems, Academic Press.

Atkinson, G. M., and R. F. Mereu (1992). The shape of ground motion attenuation curves in Southeastern Canada, *Bull. Seis. Soc. Amer.* **82,** 2014-2031.

Baker, G. E., J. Stevens, and H. M. Xu (2004). Lg group velocity: A depth discriminant revisited, *Bull. Seis. Soc. Amer.* **94,** 722-739.

Bates, D. M., and D. Watts (1988). Nonlinear regression analysis and its applications, New York : Wiley.

Benz, H. M., A. Frankel, and D. M. Boore (1997). Regional *Lg* attenuation for the continental United States, *Bull. Seis. Soc. Amer.* **87,** 606-619.

Boore, D. M., and J. Boatwright (1984). Average body-wave radiation coefficients, *Bull. Seis. Soc. Amer.* **74,** 1615-1621.

Bowman, J. R., and B. L. N. Kennett (1991). Propagation of *Lg* waves in the North Australian Craton; influence of crustal velocity gradients, *Bull. Seis. Soc. Amer.* **81,** 592-610.

Campillo, M. (1990). Propagation and attenuation characteristics of the crustal phase *Lg*, *Pure Appl. Geophys.* **132,** 1-19.

Campillo, M., J. Plantet, and M. Bouchon (1985). Frequency-dependent attenuation in the crust beneath central France from *Lg* waves; data analysis and numerical modeling, *Bull. Seis. Soc. Amer.* **75,** 1395-1411.

Chavez, D. E., and K. F. Priestley (1986). Measurement of frequency dependent *Lg* attenuation in the Great Basin, *Geophys. Res. Lett.* **13,** 551-554.

Chun, K., G. F. West, R. J. Kokoski, and C. Samson (1987). A novel technique for measuring *Lg* attenuation; results from Eastern Canada between 1 to 10 Hz, *Bull. Seis. Soc. Amer.* **77,** 398-419.

Chung, T. W., Y. K. Park, I. B. Kang, and K. Lee (2005). Crustal Q_{Lg}^{-1} in South Korea using the source pair/receiver pair method, *Bull. Seis. Soc. Amer.* **95,** 512-520.

Chung, T., and K. Lee (2003). A study of high-frequency Q_{Lg}^{-1} in the crust of South Korea, *Bull. Seis. Soc. Amer.* **93,** 1401-1406.

Erickson, D., D. E. McNamara, and H. M. Benz (2004). Frequency-dependent *Lg Q* within the continental United States, *Bull. Seis. Soc. Amer.* **94,** 1630-1643.

Fan, G. W., and T. Lay (2003a). Strong *Lg* attenuation in the Tibetan Plateau, *Bull. Seis. Soc. Amer.* **93,** 2264-2272.

Fan, G., and T. Lay (2003b). Strong *Lg* wave attenuation in the northern and eastern Tibetan Plateau measured by a two-station/two-event stacking method, *Geophys. Res. Lett.* **30,** 4.

Faraway, J. J. (2004). Linear Models with R, Chapman & Hall/CRC.

Frankel, A. (1990). Attenuation of high-frequency shear waves in the crust: measurements from New York State, South Africa, and Southern California, *J. Geophys. Res.* **95,** 17441-17457.

Goldstein, P., D. Dodge, and M. Firpo (1999). SAC2000: Signal processing and analysis tools for seismologists and engineers, in *International Handbook of Earthquake and Engineering Seismology*, Part B, Int. Geophys., vol 81B, edited by W. Lee et al., pp. 1613-1614, New York: Elsevier.

Graves, R. W., and S. M. Day (2003). Stability and accuracy analysis of coarse-grain viscoelastic simulations, *Bull. Seis. Soc. Amer.* **93,** 283-300.

Hanks, T. C., and A. C. Johnston (1992). Common features of the excitation and propagation of strong ground motion for North American earthquakes, *Bull. Seis. Soc. Amer.* **82,** 1-23.

Malagnini, L., K. Mayeda, R. Urhammer, A. Akinci and R. B. Herrmann (2007). A regional ground-motion excitation/attenuation model for the San Francisco region, *Bull. Seism. Soc. Amer.*, 97, 843-862.

Mayeda, K., L. Malagnini, W. S. Phillips, W. R. Walter, and D. Dreger (2005). 2-D or not 2-D, that is the question: A northern California test, *Geophys. Res. Lett.* **32,** L12301.

Mayeda, K., A. Hofstetter, J. L. O'Boyle, and W. R. Walter (2003). Stable and transportable regional magnitudes based on coda-derived moment-rate spectra, *Bull. Seis. Soc. Amer.* **93,** 224-239.

McNamara, D. E., T. J. Owens, and W. R. Walter (1996). Propagation characteristics of *Lg* across the Tibetan Plateau, *Bull. Seis. Soc. Amer.* **86,** 457-469.

Moore, D. S., and G. P. McCabe (2002). Introduction to the Practice of Statistics, W. H. Freeman.

Nuttli, O. W. (1973). Seismic Wave Attenuation and Magnitude Relations for Eastern North America, *J. Geophys. Res.* **78,** 876-885.

Olson, A. H., and J. G. Anderson (1988). Implications of frequency-domain inversion of earthquake ground motions for resolving the space-time dependence of slip on an extended fault, *Geophys. J. R. Astro. Soc.* **94,** 443-455.

R Development Core Team. (2006). R: A Language and Environment for Statistical Computing, R Foundation for Statistical Computing, Vienna, Austria.

Shih, X. R., K. Y. Chun, and T. Zhu (1994). Attenuation of 1-6 s *Lg* waves in Eurasia, *J. Geophys. Res.* **99,** 23-23,875.

Street, R. L., R. B. Herrmann, and O. W. Nuttli (1975). Spectral characteristics of the L_g wave generated by central United States earthquakes, *Geophys. J. R. Astro.* **41,** 51-63.

Taylor, S. R., A. A. Velasco, H. E. Hartse, W. S. Phillips, W. R. Walter, and A. J. Rodgers (2002). Amplitude corrections for regional seismic discriminants; Monitoring the Comprehensive Nuclear-Test-Ban Treaty; seismic event discrimination and identification, *Pure Appl. Geophys.* **159,** 623-650.

Venables, W. N., and B. D. Ripley (2002). Modern Applied Statistics with S, Springer, New York.

Walter, W. R., K. Mayeda, L. Malagnini, and L. Scognamiglio (2007). Regional body-wave attenuation using a coda source normalization method: Application to MEDNET records of earthquakes in Italy, *Geophys. Res. Lett.* **34,** L10308.

Wessel, P., and W. H. F. Smith (1998). New, improved version of generic mapping tools released, in American Geophysical Union, San Francisco, Vol. 79, 579.

Xie, J., R. Gok, J. Ni, and Y. Aoki (2004). Lateral variations of crustal seismic attenuation along the INDEPTH profiles in Tibet from Lg Q inversion, *J. Geophys. Res.* **109,** B10308.

Xie, J., and B. J. Mitchell (1990). Attenuation of multiphase surface waves in the Basin and Range Province; Part I, *Lg* and *Lg* coda, *Geophys.J. Int.* **102,** 121-137.

Xie, J. (2002). Lg Q in the eastern Tibetan Plateau, *Bull. Seis. Soc. Amer.* **92,** 871-876.

Xie, J. (1998). Spectral inversion of Lg from earthquakes; a modified method with applications to the 1995, western Texas earthquake sequence, *Bull. Seis. Soc. Amer.* **88,** 1525-1537.

Yang, X. N. (2002). A numerical investigation of *Lg* geometrical spreading, *Bull. Seis. Soc. Amer.* **92,** 3067-3079.

Yoshimoto, K., H. Sato, and M. Ohtake (1993). Frequency-dependent attenuation of P and S waves in the Kanto area, Japan, based on the coda-normalization method, *Geophys. J. Int.* **114,** 165-174.

University of California, Berkeley
(S.R.F., D.S.D., K.M.)

Lawrence Livermore National Laboratory
(W.R.W.)

Istituto Nazionale di Geofisca e Vulcanologia
(L.M.)

Los Alamos National Laboratory
(W.S.P.)

Table 1. Q_{Lg} measurement method parameterization for sensitivity tests

Group	Spreading exponent [γ]	Measurement bandwidth (Hz)	Epicentral distance [*r*] (km)	*Lg* velocity window (km/s)
Control	0.5	0.5 - 8	100 - 400	2.6 - 3.5
Test 1 (γ)	**0.83**			
Test 2 (Bandwidth)		**0.25 - 4**		
Test 3 (Distance)			**100 - 700**	
Test 4 (Window)				**3.0 - 3.6**

Table 2. Method summary

Method	Assumptions	Advantages	Disadvantages
CN	1. Amplitude is measured at a point where coda scattering is homogeneous in space 2. Direct wave geometrical spreading is assumed	1. Independent of source and site 2. Can use all event station paths	1. Coda may not be homogeneous, or sensitive to source and site 2. Won't work when SNR too low to measure coda
CS	1. Direct wave geometrical spreading is assumed 2. Requires an independent method (e.g. coda) to obtain source spectrum	1. Can use all event-station paths	1. Short path attenuation very dependent on geometrical spreading assumptions 2. Site effects map into Q if not known independently
TS	1. Source cancels when event to two stations azimuth is within 15° 2. Direct wave geometrical spreading is assumed	1. Independent of source	1. Paths are limited by the event-station layout 2. Site effect differences between two stations can map into *Q*
RTS	1. Path is identical when event to two stations azimuth is within 15° 2. Direct wave geometrical spreading is assumed	1. Independent of source and site	1. Paths are limited by event-station layout
SPRP	1. Path is identical when event to two stations azimuth is within a function that depends on distance. 2. Source radiation is isotropic	1. Independent of source and site	1. Least limiting of two station methods, but paths are limited to interstation

Figure 1. Events (stars) and stations (inverted triangles) used to calculate Q_{Lg} in Northern California. The great-circle paths used in the example figures for the CS, TS and RTS methods are black.

Figure 2. Q_{Lg} at station PKD measured by the coda normalization method. a) Robust regression of coda normalized *Lg* amplitudes (crosses) versus distance where the spreading exponent γ is 0.5 and the bandwidth of the measurement is in the upper right. The slope is related to Q^{-1} which is given on the left with standard error. b) Weighted regression of Q^{-1} (diamonds with standard error bars) versus frequency bandwidth midpoint, where the power-law attenuation parameters with standard deviations are given in the lower left.

Figure 3. Q_{Lg} for the path between event 1999230010618 (see Supplemental Table) and station PKD measured by the coda-source normalization method. $Q_0 f^{\eta}$ with standard error is given in the lower right.

Figure 4. Q_{Lg} measured by the two-station method for the path between stations PKD and SAO from event 1999230010618 (see Supplemental Table). The best-fit parameters are given in the lower right with standard error. Notice the $\alpha < 0$ at some points which creates a singularity when the power-law model is linearized with the log transform.

Figure 5. Q_{Lg} measured by the reverse two-station method for the path between stations PKD and SAO for events 1999230010618 and 2004273225453 (see Supplemental Table). The best-fit parameters are given in the lower right with standard error.

Figure 6. Q_{Lg} for the path between stations PKD and SAO as measured by the source-pair/receiver-pair method. a) Robust regression of *Lg* amplitude ratios (crosses) versus effective distance where the spreading rate γ is 0.5, and the bandwidth of the measurement is in the upper right. The slope is related to Q^{-1}, which is given in the lower left with standard error. b) Weighted regression of Q^{-1} (diamonds with standard error bars) versus frequency bandwidth midpoint, where the power-law attenuation parameters with standard deviations are given in the lower left. The bandwidth between 1-2 Hz produced a very small slope, and thereby unrealistic Q^{-1}, so its value is not regressed and is absent in b).

Figure 7. Method comparison. a) Map (same region as Figure 1) of the data subset used in the comparison analysis. Data are in a small region near the San Francisco Bay Area, primarily along the Franciscan block. b) Power-law parameters associated with each method; coda normalization (CN), coda-source normalization (CS), two-station (TS), reverse two-station (RTS), and source-pair/receiver-pair (SPRP). The empirical 95% confidence regions for each method are given. The intersecting region is shaded grey.

Figure 8. Parameterization effects of the coda-normalization method. a) Power-law parameters (Q_0, η) for each choice of parameterization and the standard error region using the example station as in Figure 7. b) Results of significant difference in pairwise comparisons between the control parameterization and tests (similar symbol as panel a) at all stations. The box in the upper right gives percentage of measurements that had a significant difference and the symbols are at

the median difference (ΔQ_0, $\Delta\eta$) with upper (3rd quartile) and lower (1st quartile) bounds given by the bars.

Figure 9. Parameterization effects of the coda-source normalization method. See Figure 8 for explanation, where a) is the same path as in Figure 3 and b) is for all paths.

Figure 10. Parameterization effects of the two-station method. See Figure 8 for explanation, where a) is the same interstation path as in Figure 4 and b) is for all interstation paths.

Figure 11. Parameterization effects of the reverse two-station method. See Figure 8 for explanation, where a) is the same interstation path as in Figure 5 and b) is for all interstation paths.

Figure 12. Parameterization effects of the source-pair/receiver-pair method. See Figure 8 for explanation, where a) is the same interstation path as in Figure 6 and b) is for all interstation paths.

Figure 13. Comparison of power-law parameters for each interstation path that involves either station BRK (abscissa) or BKS (ordinate) measured with the TS method. Standard error bars are given for all parameters. If parameter values are similar they would fall along the grey line.

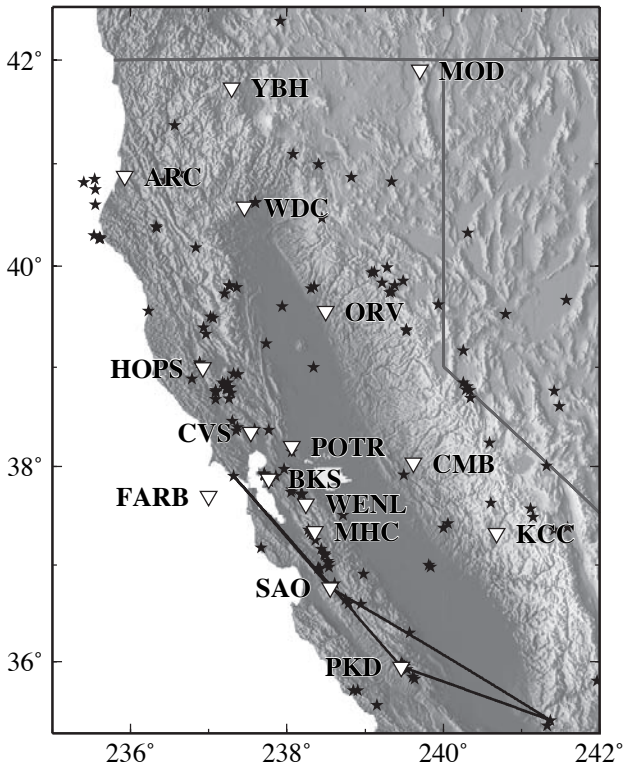

Figure 1. (1-column B/W)
Ford et al., 2007
Version 4

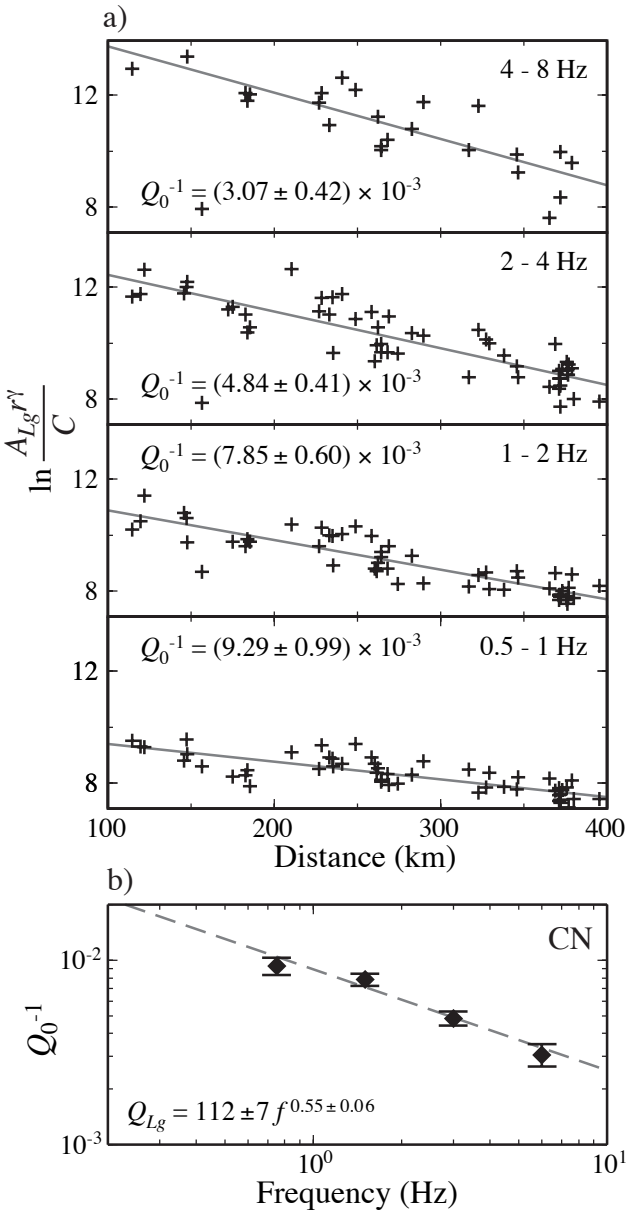

Figure 2. (1-column B/W)
Ford et al., 2007
Version 6

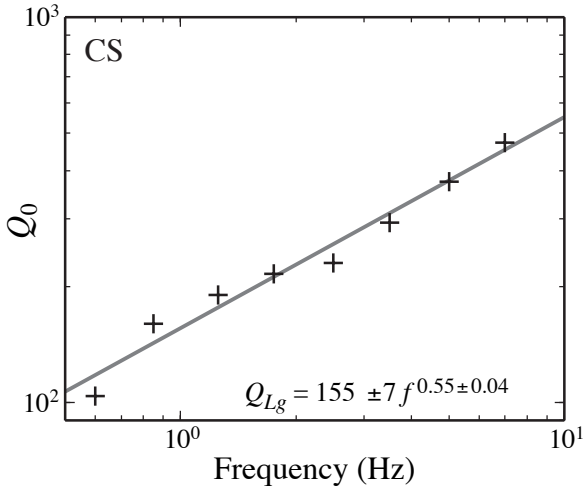

Figure 3. (1-column B/W)
Ford et al., 2007
Version 6

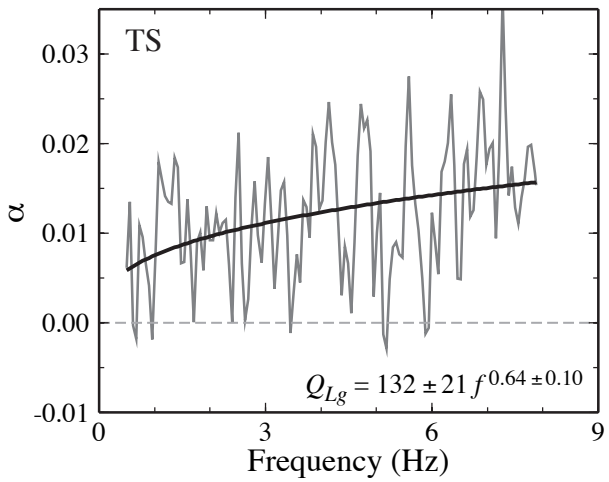

Figure 4. (1-column B/W)
Ford et al., 2007
Version 6

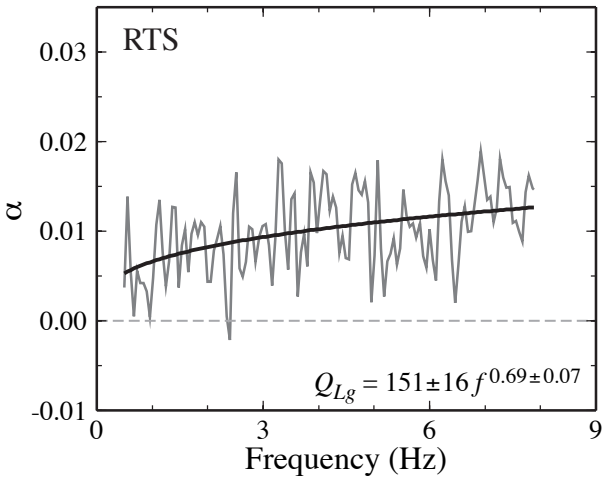

Figure 5. (1-column B/W)
Ford et al., 2007
Version 6

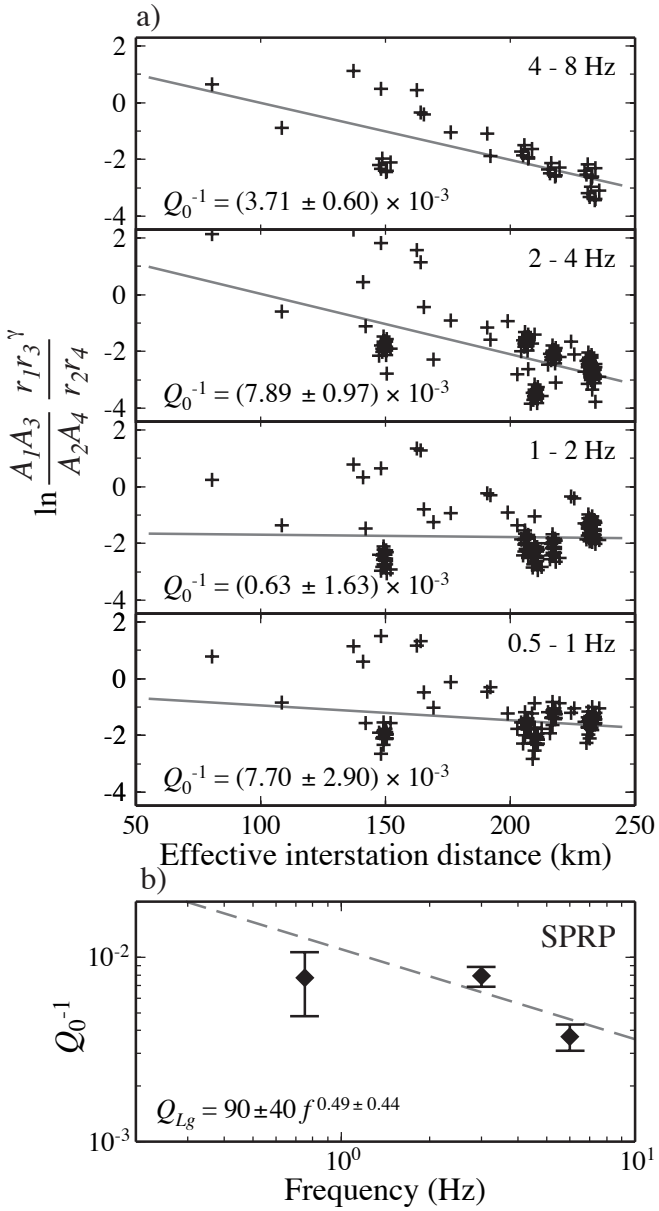

Figure 6. (1-column B/W)
Ford et al., 2007
Version 6

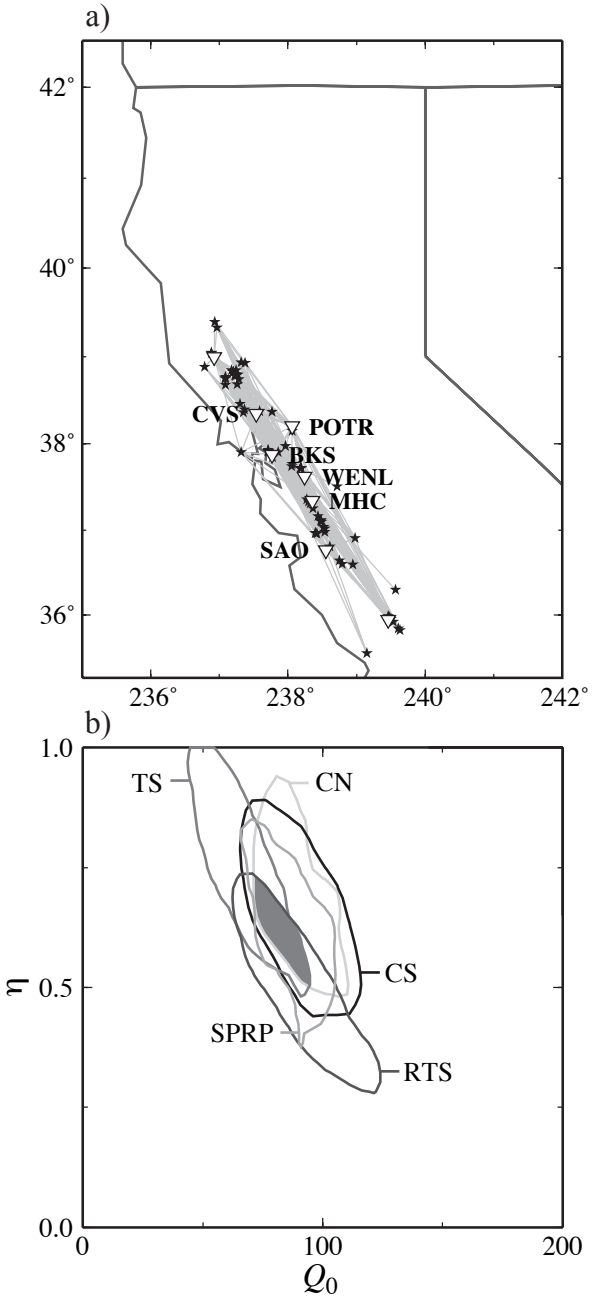

Figure 7. (1-column B/W)
Ford et al., 2007
Version 6

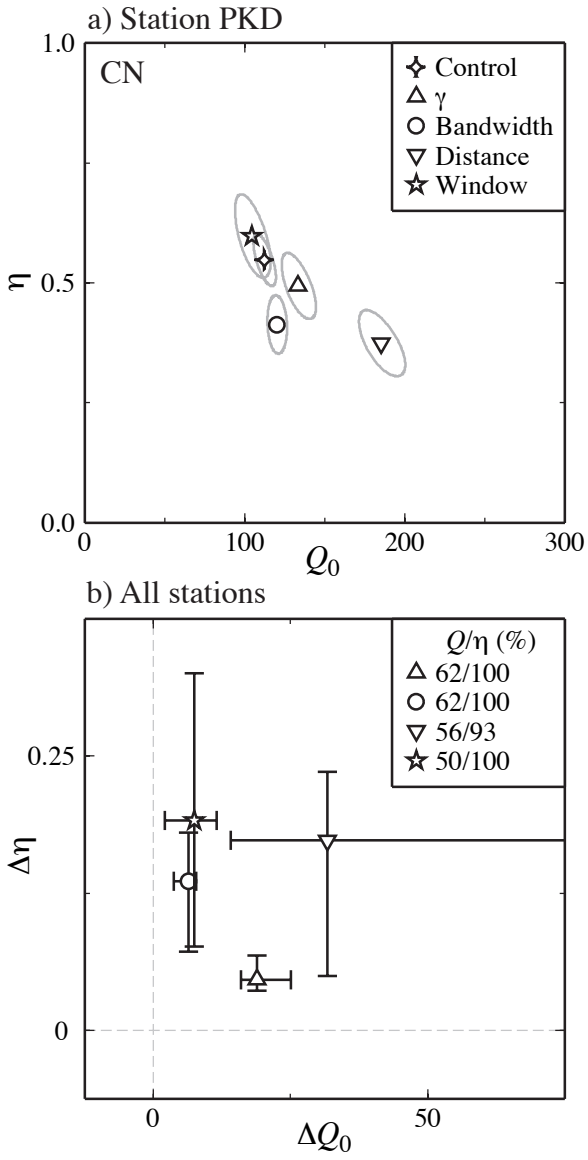

Figure 8. (1-column B/W)
Ford et al., 2007
Version 6

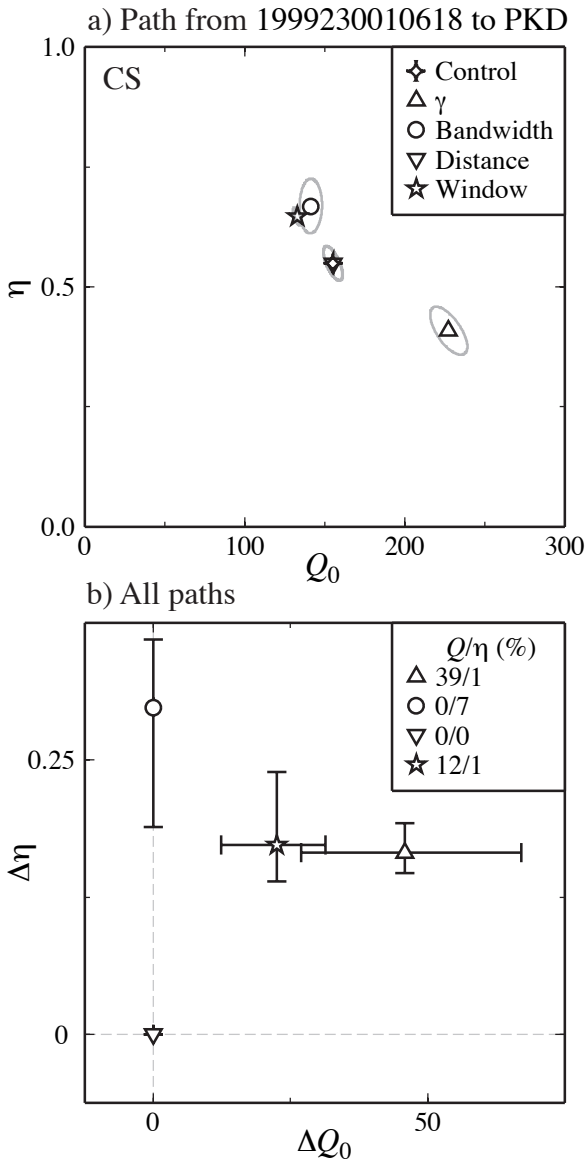

Figure 9. (1-column B/W)
Ford et al., 2007
Version 6

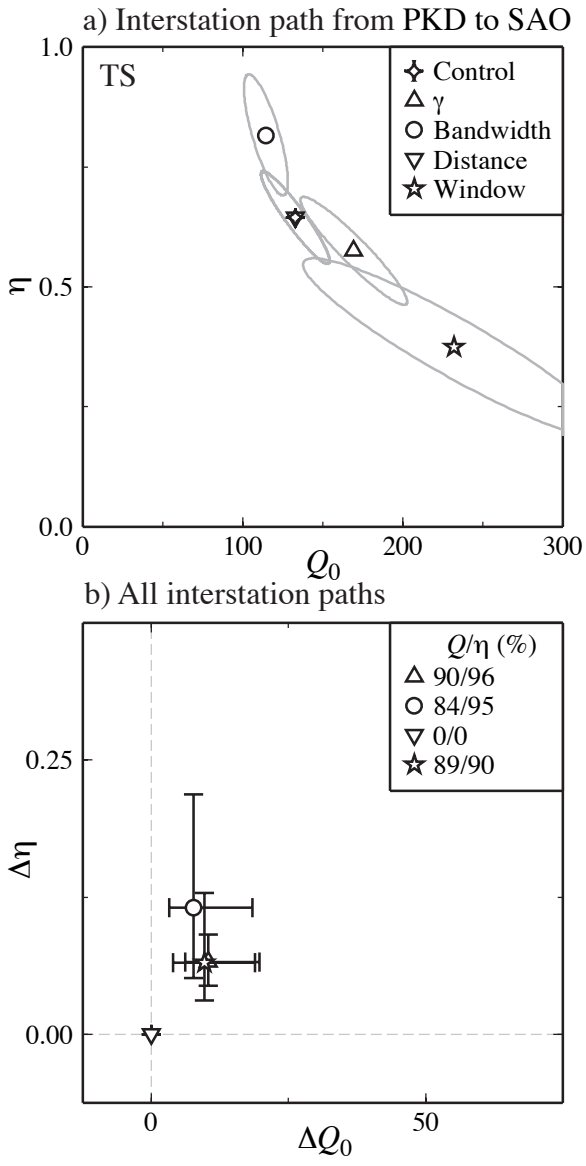

Figure 10. (1-column B/W)
Ford et al., 2007
Version 6

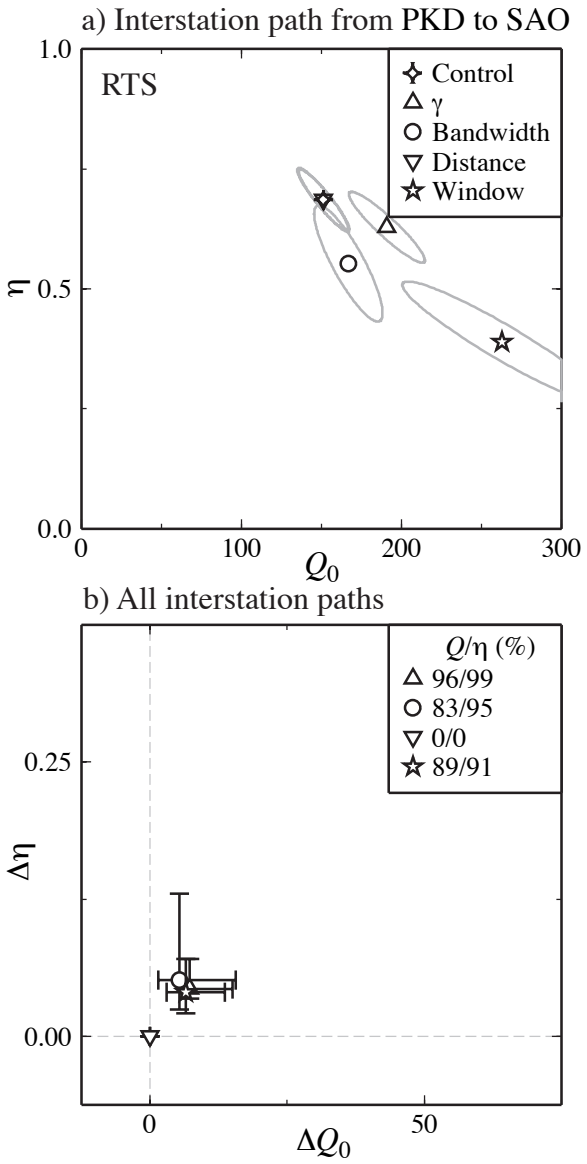

Figure 11. (1-column B/W)
Ford et al., 2007
Version 6

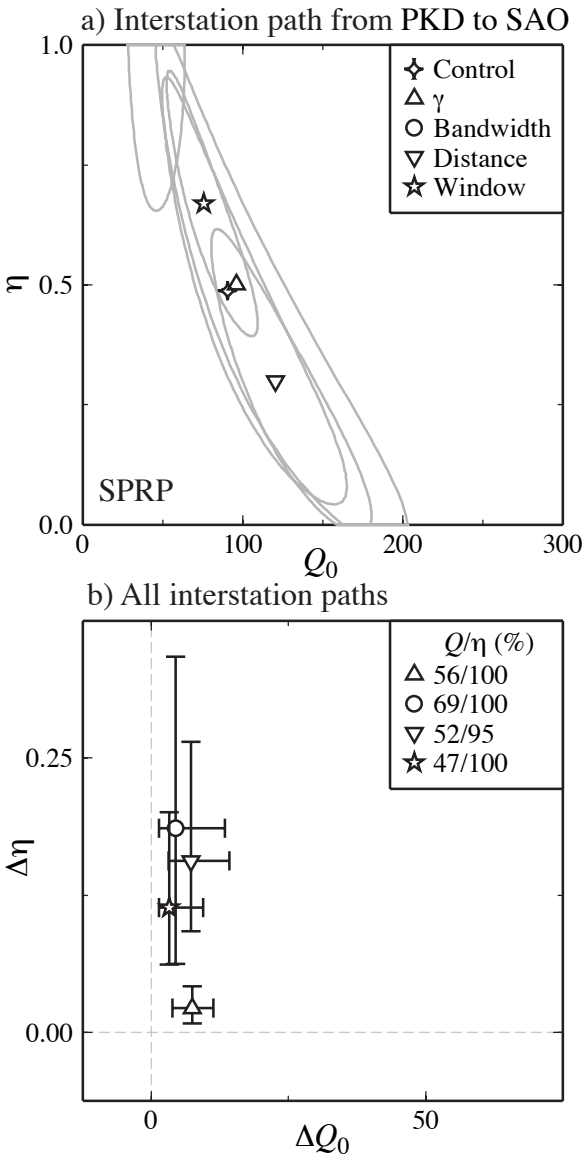

Figure 12. (1-column B/W)
Ford et al., 2007
Version 6

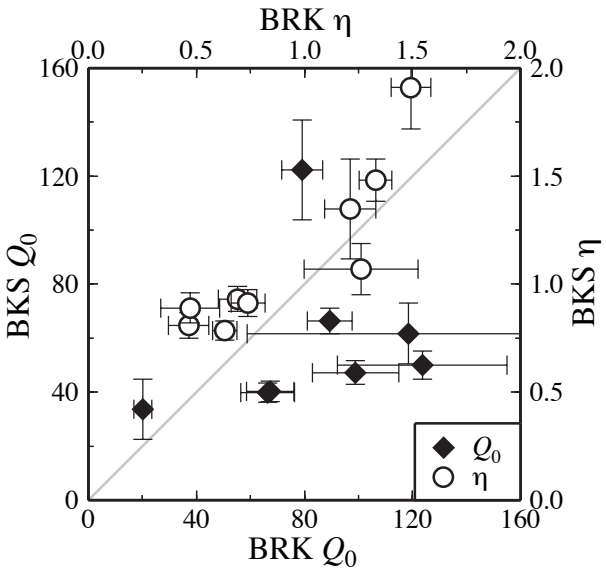

Figure 13. (1-column B/W)
Ford et al., 2007
Version 6